SUN2 Modulates the Propagation of HSV-1

Kendra Cruz-Palomar,[a] Josiane Hawkins,[a] Catherine Vandal,[a] Jordan Quenneville,[b] Étienne Gagnon,[b,c] Roger Lippé[a,d]

[a]Centre de Recherche du CHU Sainte-Justine, Montréal, Québec, Canada
[b]Institute for Research in Immunology and Cancer, Université de Montréal, Montréal, Québec, Canada
[c]Department of Microbiology, Infectiology and Immunology, Université de Montréal, Montréal, Québec, Canada
[d]Department of Pathology and Cell Biology, Université de Montréal, Montréal, Québec, Canada

Kendra Cruz-Palomar and Josiane Hawkins contributed equally to this article. Kendra Cruz-Palomar initiated this work and was listed at the first of the two coauthors.

ABSTRACT Herpesviruses assemble new viral particles in the nucleus. These nucleocapsids bud through the inner nuclear membrane to produce enveloped viral particles in the perinuclear space before fusing with the outer nuclear membrane to reach the cytoplasm. This unusual route is necessary since viral capsids are too large to pass through nuclear pores. However, the transient perinuclear nucleocapsids (250 nm in diameter) are also larger than the width of the perinuclear space (30 to 50 nm). Interestingly, linker of the nucleoskeleton and cytoskeleton (LINC) components SUN and KASH connect the inner and outer nuclear membranes and regulate their spacing. Previous work by others on the related pseudorabies virus and human cytomegalovirus showed that they functionally interact with SUN proteins. To clarify the role of SUN proteins, we explored their impact on herpes simplex virus 1 (HSV-1), another herpesvirus. Using dominant negative SUN mutants and RNA interference, we show that HSV-1 propagation is dependent on the LINC complex. In contrast to pseudorabies virus, SUN2 disruption by either approach led to increased HSV-1 extracellular viral yields. This SUN2 dependency may be linked to its greater impact on perinuclear spacing in infected cells compared to SUN1. Finally, the virus itself seems to modulate perinuclear spacing.

IMPORTANCE The large size of herpesviruses prevents them from travelling across the nuclear pores, and they instead egress across the two nuclear membranes, generating short-lived enveloped perinuclear virions. This poses a challenge as the perinuclear space is smaller than the virions. This implies the separation (unzipping) of the two nuclear membranes to accommodate the viral particles. The LINC complex bridges the two nuclear membranes and is an important regulator of perinuclear spacing. Work by others hint at its functional implication during pseudorabies virus and cytomegalovirus propagation. The present study probes the importance for HSV-1 of the SUN proteins, the LINC components found in the inner nuclear membrane. Using dominant negative constructs and RNA interference (RNAi), the data reveal that SUN2 exhibits antiviral propriety toward HSV-1, as disrupting the protein leads to increased viral yields. This is in contrast with that reported for pseudorabies and suggests that differences among herpesviruses may, once again, prevail.

KEYWORDS SUN, KASH, LINC, herpes, HSV, egress

Herpes simplex virus 1 (HSV-1) is an alphaherpesvirus primarily associated with cold sores and more occasionally with genital herpes, virus-induced blindness, encephalitis, and congenital conditions (1–3). Viral gene expression, genome duplication, and capsid assembly all occur within the nucleus. Given that the newly assembled nucleocapsids (125 nm in diameter) are too large to travel across the nuclear pores (40-nm diameter), new capsids containing the viral genome instead pass through the two

nuclear membranes to be released into the cytoplasm, where they will acquire most of the tegument and its final envelope before being released by exocytosis (4–7). During their passage through the nuclear membranes, virions thus undergo an envelopment-deenvelopment process by which they first acquire a primary envelope by budding through the inner nuclear membrane (INM) to reach the perinuclear space (PNS). These transient perinuclear virions then fuse their envelope with the outer nuclear membrane (ONM) to release naked nucleocapsids into the cytoplasm. The precise mechanism governing HSV-1 nuclear egress has yet to be elucidated, but the viral kinase pUS3 as well as the nuclear egress complex (pUL31 and pUL34 viral proteins) are clearly implicated (8–12). There is also evidence that the viral proteins VP16 and pUL51 as well as the host proteins TorsinA, protein kinase C, p32, protein kinase D, Nir2, and GGA1 may also be implicated (13–18). However, one significant issue is how the tightly regulated perinuclear space (30 to 50 nm) (19–21) can accommodate the larger viral particles. Numerous electron microscopy (EM) studies have shown that the virus causes the separation of the two nuclear membranes but the mechanistic details of that perturbation remains to be clarified (22–26).

The linker of the nucleoskeleton and cytoskeleton (LINC) complex is located in the nuclear membranes, spanning through the PNS. There are two families of proteins forming this complex as follows: SUN (Sad1, UNC-84) and KASH (Klarsicht, ANC-1, SYNE homology; also referred to as nesprins) (27). Both SUN and KASH proteins are transmembrane proteins anchored, respectively, to the inner and outer nuclear membrane. SUN proteins interact with the nuclear lamina via their nucleoplasmic domain. Meanwhile, KASH proteins interact with the cytoskeleton through their cytoplasmic domain. Finally, SUN and KASH conserved domains interact together in the PNS, forming a bridge between the two nuclear membranes (28). Five SUN proteins have been described, among which SUN3 to SUN5 are testis specific (29), while SUN1 and SUN2 are ubiquitously expressed and interact with the six KASH proteins reported so far (30, 31). The LINC complex is vital for several functions, including nuclear morphology and positioning, mechanotransduction, and the maintenance of a constant PNS (27, 32, 33). The LINC complex has also been involved in the replication of human immunodeficiency virus (HIV), human cytomegalovirus (HCMV), and pseudorabies virus (PrV), the last two being herpesviruses. Interestingly, it has been reported that SUN1 and SUN2 modulate HIV nuclear delivery (34), whereas HCMV reduces both SUN1 and SUN2 protein levels, allowing separation of the nuclear membranes, thereby facilitating the exit of nucleocapsids from the nucleus to the cytoplasm (35). Furthermore, overexpression of a dominant negative form of SUN2 alters the perinuclear space and decreases the spread of PrV (36). It is not clear, however, if the LINC complex also regulates the spread of other herpesviruses, such as HSV-1.

Focusing on SUN1 and SUN2, we probed whether their disruption impacts HSV-1 egress. Using RNA interference and dominant negative constructs expressing green fluorescent protein (GFP)-tagged luminal portions of SUN1 or SUN2, we show that HSV-1 egress is modulated by SUN2 but not SUN1. However, unlike PrV, where SUN2 inhibition reduces viral yields, SUN2 inhibition stimulated HSV-1 extracellular titers. This correlates with a greater impact of SUN2 on perinuclear spacing in infected cells.

RESULTS

Dominant negative SUN1 or SUN2 overexpression has a minimal impact on HSV-1 propagation in the 143B human cell line. To assess the potential implication of the LINC complex in the HSV-1 viral cycle, we initially transfected 143B cells with the pGFP-luSUN1 and pGFP-luSUN2 plasmids as previously done for PrV (36). These cells were selected, as they are susceptible to HSV-1 yet better resist the reorganization of their intracellular organelles when infected (37, 38). They are therefore very useful to monitor HSV-1 egress (18, 39–42). However, the transfection of 143B cells revealed a low rate of transfected cells that were also infected, making it difficult to quantitatively assess the impact of the constructs on viral egress. Establishing 143B stable cell lines by clonal selection also proved challenging since the exogenous genes appeared to

largely be unstable, presumably because the LINC complex is important to the cells. For these reasons, we resorted to inducible cell lines. We therefore produced lentiviruses coding for doxycycline (DOX) inducible GFP-luSUN1 or GFP-luSUN2 and then transduced 143B cells with these lentiviruses. Following their selection for puromycin resistance over 2 weeks, the cell lines were treated with doxycycline for 48 h and analyzed by flow cytometry to monitor the efficacy of the transduction. Figure 1 shows that the expression of the GFP-luSUN1 or GFP-luSUN2 was, as anticipated, responsive to DOX induction, while wild-type 143B cells were naturally insensitive to the DOX treatment and only had background levels of fluorescence. However, a significant proportion of the cells seemingly lost the exogenous genes despite the puromycin selection. For this reason, freshly induced cells were always sorted prior to infecting them in subsequent experiments.

Given that HSV-1 can shut down the expression of numerous host genes (43–50), we next explored the impact of the virus on the exogenous expression of the SUN constructs. Hence, presorted DOX-induced cells were infected for 12 h and GFP levels monitored by immunofluorescence (IF) and flow cytometry (Fig. 2). Cells were also labeled with an antibody targeting the ICP4 viral protein to monitor the infection. As expected, only infected cells were ICP4 positive, and once again GFP-luSUN expression was induced by DOX (Fig. 2A). Under these conditions, 91% and 93% of the cells expressed GFP-luSUN1 or GFP-lu.SUN2, respectively. Overexpression of these constructs led to both a cytoplasmic and nuclear envelope staining in mock and infected cells (Fig. 2A). This was anticipated, as the GFP-lu.SUN constructs lack the transmembrane domain that targets the endogenous SUN1 and SUN2 proteins to the nuclear envelope (27, 51–53). However, the lu-SUN-dominant negative mutants still reach the nuclear envelope (as shown in Fig. 2A) and have previously been shown to uncouple the LINC complex, displace nesprins, and enhance the spacing between the two nuclear envelopes (27, 36, 43). Quantification of SUN1 expression by flow cytometry indicated that the mean fluorescence intensities (MFI) were respectively 254 (no DOX/uninfected), 1,416 (no DOX/HSV), 14,380 (DOX/uninfected), and 19,847 (DOX/HSV). For SUN2, the MFI values were 529, 1,579, 24,252, and 32,135, respectively (Fig. 2B). We conclude that while HSV-1 somewhat stimulated the expression of the dominant constructs barely above basal levels (3- to 5-fold) compared to uninfected cells, the constructs were strongly induced by DOX (up to 60-fold). In this scenario, it was thus possible to access the impact of these dominant constructs on viral yields. Plaque assays were therefore performed on fluorescence-activated cell sorter (FACS) sorted GFP-luSUN1 or GFP-luSUN2 inducible 143B cells in the presence or absence of DOX as well as control cells transduced by a lentivirus expressing mCherry (LentiCTL) (see Materials and Methods) and subsequently infected with HSV-1. To our surprise, no significant effect was recorded over three independent experiments. For nontransduced 143B cells, total extracellular viral yields were 8.74×10^4 PFU For SUN1-expressing cells, and yields were, respectively, 6.73×10^4 PFU and 7.96×10^4 PFU with or without DOX induction (Fig. 3). Similarly, for SUN2, we did not observe any difference between the values obtained in the presence or absence and of induction (7.20×10^4 PFU and 7.23×10^4 PFU, respectively).

Dominant negative SUN2 overexpression in RK13 cells stimulates viral propagation. Klupp and colleagues (36) previously reported that GFP-luSUN2 overexpression in the RK13 rabbit cell line reduced the yields of PrV, a related herpesvirus of the alphaherpesvirus family. We therefore evaluated if RK13 cells overexpressing the very same GFP-luSUN1 or GFP-luSUN2 constructs, graciously provided by the Mettenleiter laboratory, supported HSV-1 propagation as well as the wild-type RK13 cell line. FACS analyses of these RK13 cell lines also revealed some instability of the constructs, particularly for GFP-luSUN2, which was nearly all GFP negative (Fig. 4A, left). As for 143B cells, we therefore sorted GFP-positive cells, passaged them, and subsequently infected them. Reanalysis of these sorted and infected cells by flow cytometry indicated that all GFP-lu.SUN1 cells remained GFP positive, while it was 86% for the GFP-lu.SUN2 (Fig. 4B), albeit evidence for luSUN2 loss was once again
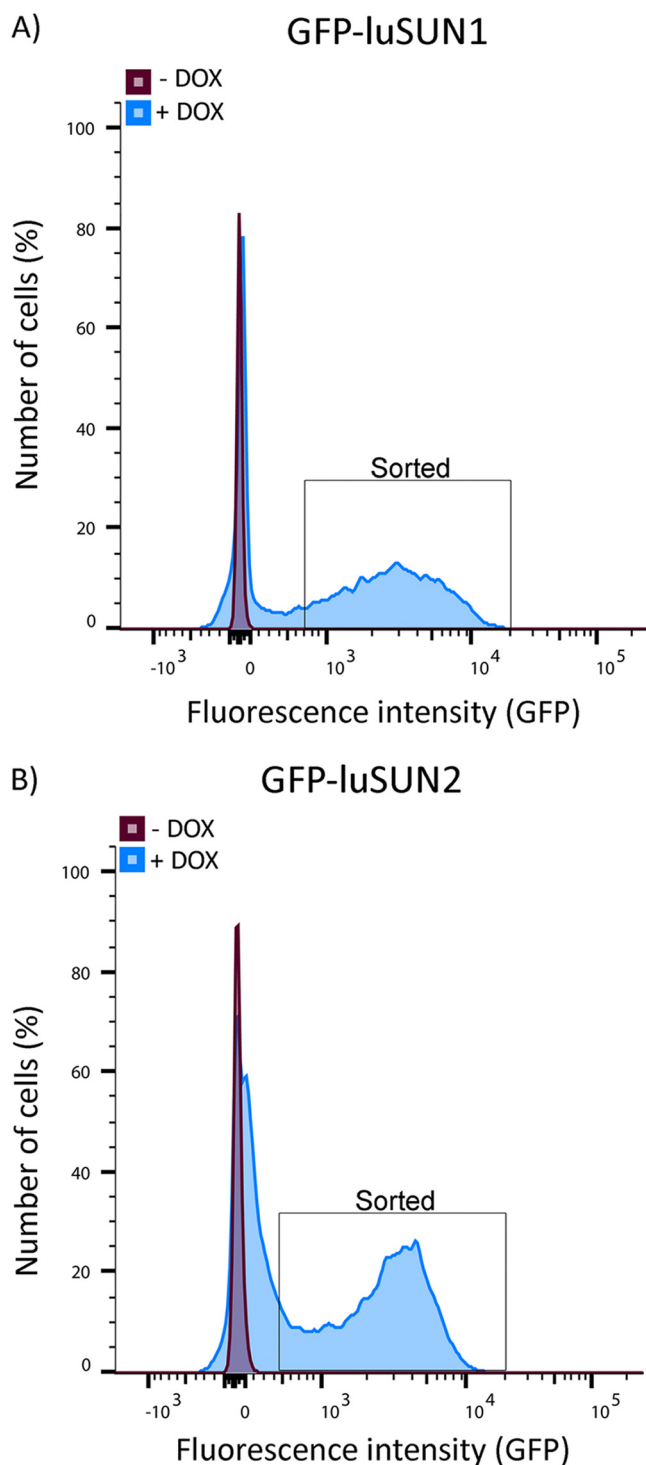
FIG 1 GFP-luSUN1 and GFP-luSUN2 inducible cell lines. The 143B GFP-luSUN1 and GFP-luSUN2 cell lines were induced for 24 h with 1 μg/mL doxycycline (DOX) (in light blue). GFP-positive cells were sorted by FACS, using corresponding non-DOX-exposed cells (in purple) as negative control (143B GFP-luSUN1 or 2, respectively). Cells recovered from FACS sorting (GFP-positive) were placed in culture and used for the subsequent experiments (*n* = 3).

apparent after only a few passages (Fig. 4A, lower right). Upon infection of freshly FACS sorted cells with HSV-1, viral yields were therefore measured. The data indicated that luSUN2 modestly and reproducibly impacted HSV-1 propagation but enhanced it rather than reducing it as reported for PrV (36). Analysis of four independent experiments revealed
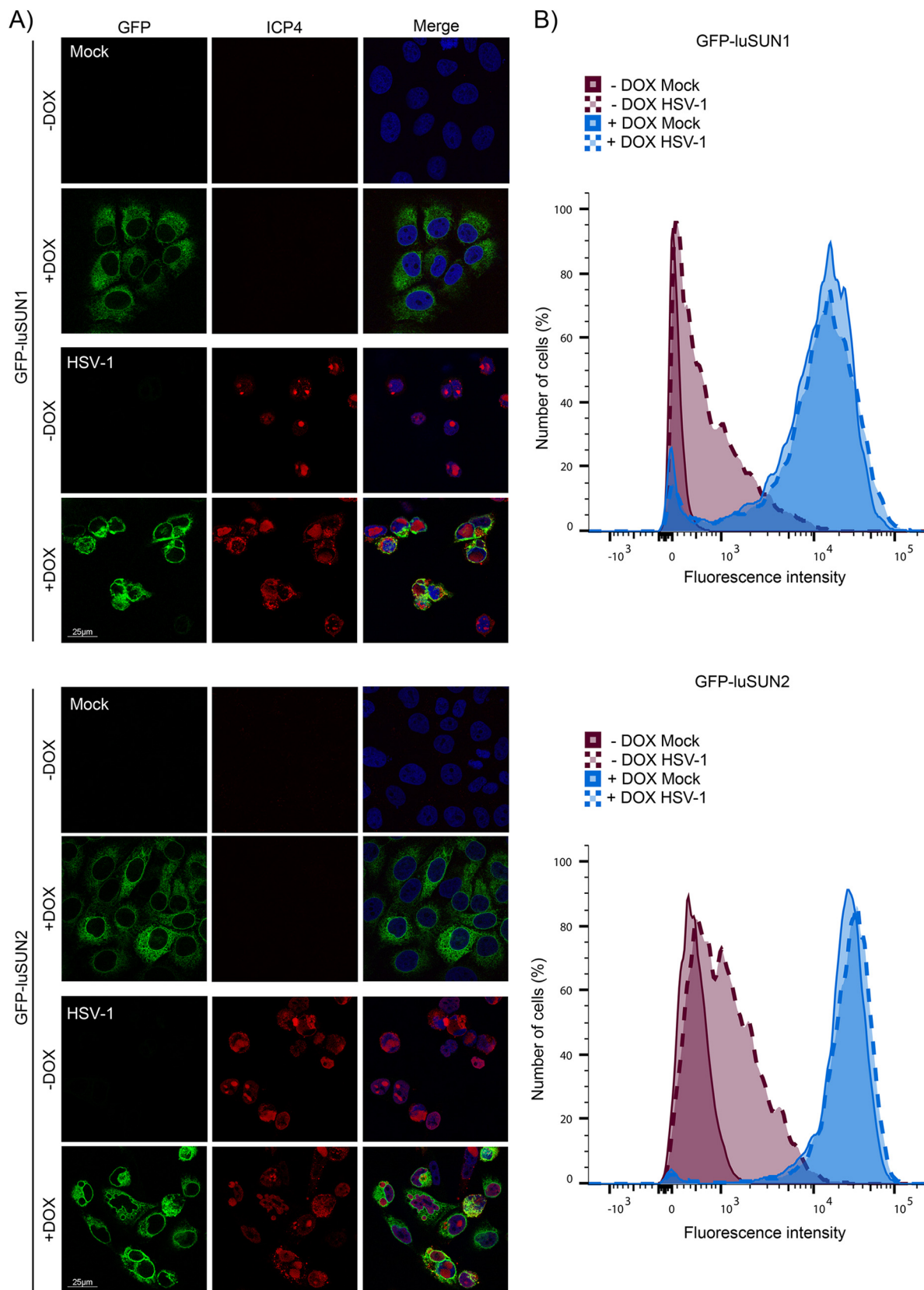
FIG 2 143B inducible cell lines are susceptible to HSV-1 infection. (A) 143B sorted cell lines were cultured on coverslips and induced or not by DOX and examined by fluorescence microscopy. (B) Sorted 143B cells were induced (blue) or not (purple) with DOX for 24 h and infected with HSV-1 with an MOI of 2 or mock treated (no virus). Twelve hours after infection, cells were recovered for analysis by FACS ($n = 3$).
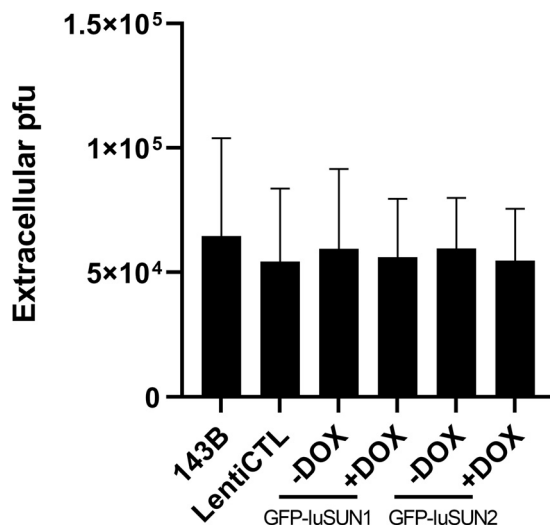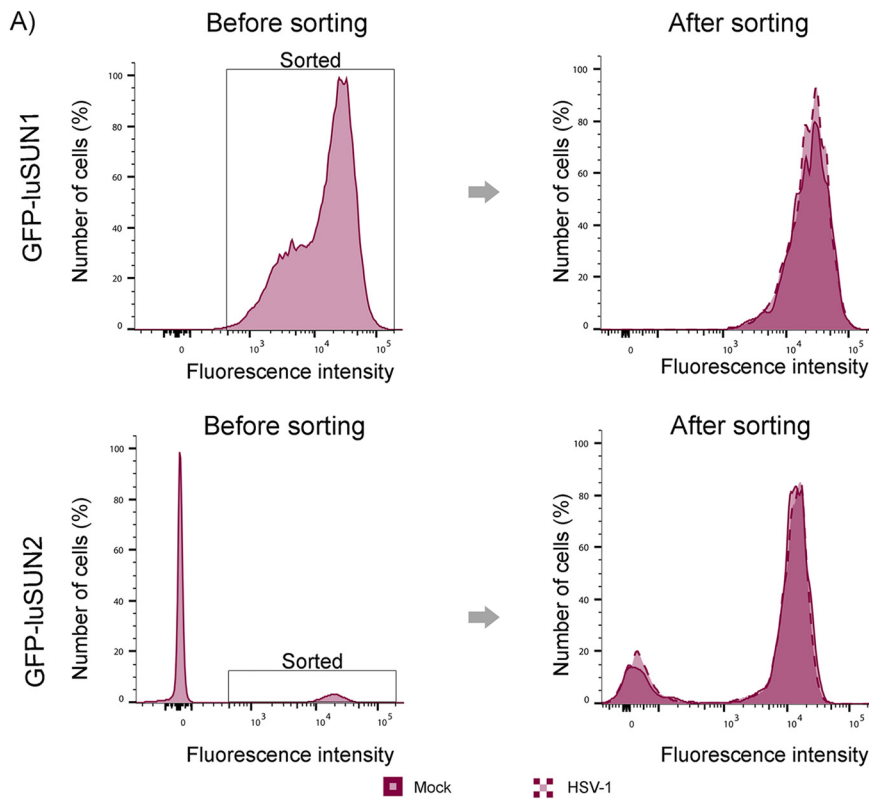
FIG 3 Overexpression of luminal portion of SUN proteins in the 143B inducible cell lines does not impact viral yields. Upon 24-h induction of the 143B GFP-luSUN1 and GFP-luSUN2 cell lines with DOX followed by a 12-h infection with HSV-1 at an MOI of 2, the supernatant was collected and titrated on Vero cells. 143B are wild-type control cells that did not undergo lentiviral transduction, whereas the LentiCTL were cells that were transduced by a lentivirus expressing mCherry. Error bars represent the standard error of the mean (SEM). No statistical differences were noted ($n = 3$).

that RK13 and RK13 GFP-luSUN1 cells, respectively, released 1.06×10^5 PFU and 8×10^4 PFU (Fig. 5). In contrast, the RK13 GFP-luSUN2 cell line yielded 2.97×10^5 PFU, a 3-fold increase that reached statistical significance ($P = 0.0011$).

RK13 cells express far more luSUN1 and luSUN2 than 143B cells. The lack of effect of SUN overexpression in 143B cells but a clear phenotype in RK13 cells was initially puzzling. Given the instability of the luSUN constructs in both cell types, we opted to compare their SUN protein levels. We first used a GFP antibody to specifically monitor the exogenously expressed proteins by Western blotting (WB). Figure 6A shows that RK13 expressed five times more luSUN1 or luSUN2 than 143B cells (normalized to gamma tubulin), which could explain why HSV-1 propagated normally in SUN overexpressing 143B cells. These constructs had no impact on the expression of the endogenous SUN mRNAs, as probed by Western blotting using SUN antibodies (Fig. 6B). Please note that the epitope recognized by the SUN1 antibody is absent in the truncated GFP-lu.SUN1 chimera, while the SUN2 antibody detects both endogenous and exogenous proteins, which unfortunately have similar masses. Thus, the SUN2 blots confirm that overexpression of GFP-lu.SUN1 or the Lenti-control expressing mCherry has no impact on SUN2 protein levels and that SUN2 is strongly enhanced in the GFP-lu.SUN2 cell line upon induction, while endogenous SUN1 is unaltered under all conditions. In an attempt to circumvent this low level of expression, we first induced 143B cells (±DOX) for 24 h, then infected them for 12 h, and finally FACS sorted them into two populations, i.e., those expressing a low level of luSUN1 or luSUN2 and those expressing a high level of the proteins (Fig. 7A, low and high populations). We then measured intracellular viral yields immediately without further expansion of the cells (Fig. 7B). Average yields over four independent experiments for luSUN1 were 2.99×10^5 PFU for uninduced cells and 1.34×10^5 PFU or 3.45×10^5 PFU for low or high expressers, respectively. Similar viral yields were obtained in the case of 143B luSUN2 cells (2.94×10^5 PFU [uninduced], 1.08×10^5 PFU [low], 3.26×10^5 PFU [high]). Neither of these populations showed a significant difference between them in terms of viral yields or compared to those of 143B untransduced cells, which gave a viral yield of 2.73×10^5 PFU. Western blot analyses indicated that the levels of expression of sorted 143B high expressers for both luSUN1 and luSUN2 remained well below that of the RK13 cell lines (Fig. 7C). It thus seemed that only very high levels of the dominant negative luSUN2 construct could efficiently impact HSV-1 propagation or that, alternatively, SUN2 only affected HSV-1 production in RK13 cells.
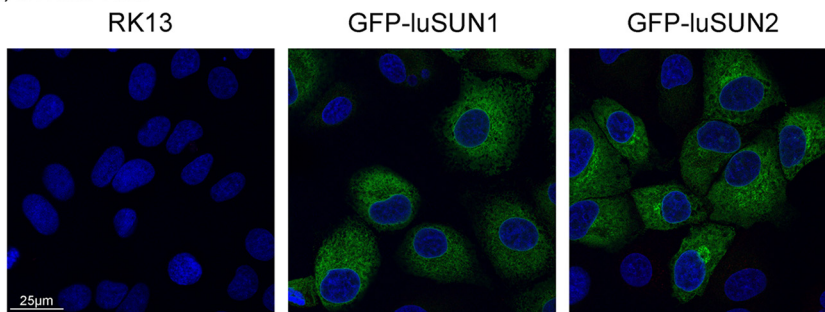
FIG 4 Analysis of stable RK13 cell lines. (A) RK13 GFP-luSUN1 or SUN2 cells were sorted by FACS (left). GFP-positive cells were recovered, cultured, and then infected with HSV-1 at an MOI of 2 for 9 h and reanalyzed by FACS analysis (right). (B) In parallel, RK13 sorted cell lines were seeded on coverslips and observed by microscopy using Hoechst to label the cell nuclei (blue). The left panel represents RK13 cells that do not overexpress the SUN1 or SUN2 dominant mutants. ($n = 3$).

Inhibition of SUN2 by RNA interference in 143B cells stimulates viral propagation. To ascertain if SUN2 is also participating in the propagation of HSV-1 in 143B cells, we used an alternative approach to block SUN2 using RNA interference. In parallel, we also targeted SUN1 and used a nontargeting reagent as control (dsiCTL). Figure 8A shows that the RNA interference (RNAi) reagents targeting endogenous SUN1 or SUN2 were specific for their respective target as monitored by Western blotting, giving an average reduction of 78% and 93% in SUN1 or SUN2 protein levels when treated with the corresponding RNAi (average of three independent experiments). Importantly, these conditions minimally impacted cell viability compared to cells treated with a control RNAi (Fig. 8B). Upon infection of 143B cells treated with control RNAi or that targeting SUN1, normal levels of HSV-1 were noted in the extracellular media (average of 7.50×10^5 and 4.33×10^5 PFU, respectively, over three independent experiments) (Fig. 8C). In contrast, the knockdown of SUN2 stimulated viral yields (4.42×10^6 PFU or an approximately 6-fold increase over the control RNAi), in agreement with the
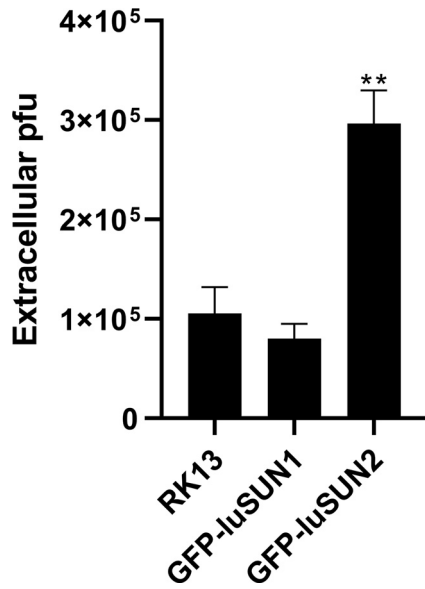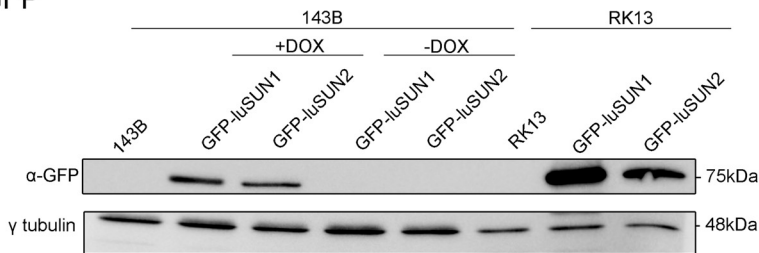
FIG 5 Overexpression of the SUN2 dominant negative mutant has a proviral effect in RK13 cells. RK13 sorted cells (wild-type RK13 or that overexpressing the SUN1 or SUN2 dominant mutants) were infected by HSV-1 at an MOI of 2 for 12 h. The supernatant was collected and titrated on Vero cells. Error bars represent SEM. Statistical analyses were done by one-way ANOVA with Dunnett multiple comparisons (**, $P \leq 0.01$) ($n = 4$).

inhibition of SUN2 with the GFP-luSUN2 dominant negative construct in RK13 cells with only a modest increase when both SUN1 and SUN2 were targeted (4.90×10^6 PFU). We conclude that the perturbation of SUN2 stimulates HSV-1 viral yields in both 143B and RK13 cells, with no evidence thus far of an implication by SUN1, and that RNAi is a better mean to knock out SUN2 in 143B cells.
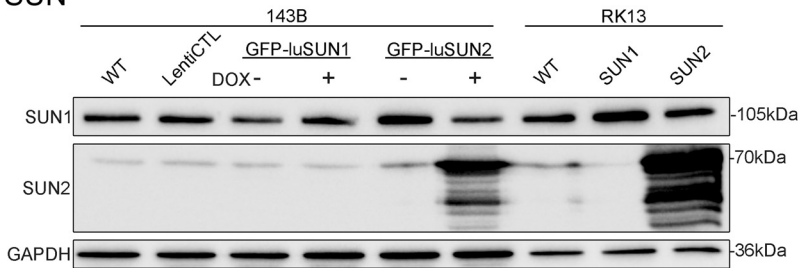

FIG 6 Dominant negative SUN1 or SUN2 expression is much lower in the 143B inducible cell lines. 143B and RK13 cells overexpressing mCherry (LentiCTL), the dominant negative (exogenous) forms of SUN1 or that for SUN2 were analyzed by Western blotting by using GFP (A) or SUN-specific antibodies (B) to probe endogenous proteins. In the case of 143B GFP-luSUN1 or SUN2, the cells were first induced or not for 24 h with 1 μg/mL DOX. Tubulin and GADPH served as loading controls. Note the SUN1 antibody only recognizes the endogenous protein while the SUN2 antibody recognizes both endogenous and exogenous proteins, which unfortunately have similar masses ($n = 3$ for all blots).
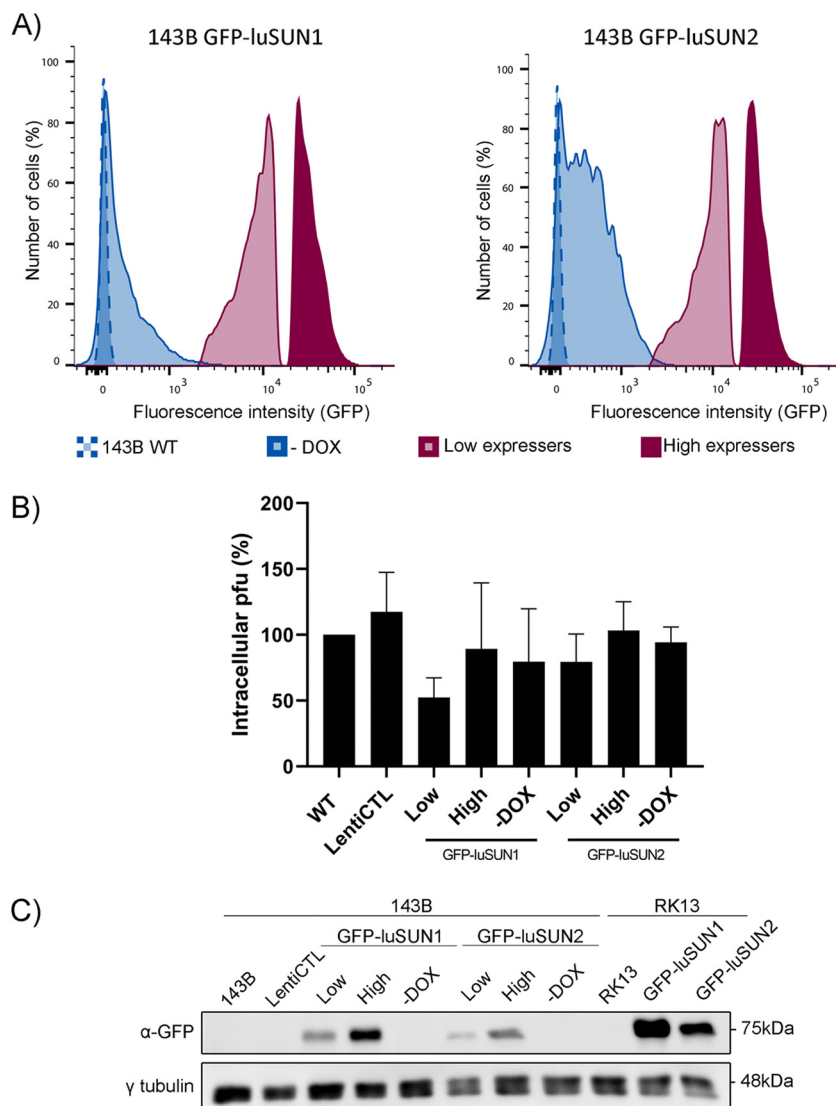
FIG 7 The level of expression of dominant negative SUN proteins on the inducible 143B cell lines does not influence the propagation of the virus. (A) 143B cells were induced (shades of red) or not (shades of blue) as described above and subsequently infected with HSV-1 with an MOI of 2 for 12 h. The infected cells were collected for FACS sorting. GFP-positive cells were recovered in two different populations, low (light red) or high (dark red) expressers. The noninduced (−DOX), nontransduced (wild-type 143B), or mCherry control cells were not sorted. An equal number of cells were recovered in each case. (B) Infected cells sorted in panel A were used to perform plaque assays on Vero cells. No statistically significant differences were found ($n = 3$). (C) Western blot of 143B sorted cells in panel A and the RK13 stable cell lines. The proteins of interest were detected with anti-GFP (GFP-luSUN proteins) or anti-tubulin (loading control) antibodies. 143B and RK13 represent cells that do not express mutant forms of SUN1 or SUN2. Error bars represent the SEM. Statistical analysis were done by one-way ANOVA ($n = 3$).

Targeting the SUN proteins disrupts perinuclear spacing and promotes viral nuclear egress. Thus, far, the data were consistent with the increased spread of HSV-1 in both 143B and RK13 cells when SUN2 function was efficiently abrogated. Since SUN proteins associate with KASH proteins through their luminal domains, we reasoned that overexpression of the dominant SUN constructs would perturb the LINC complex. To probe the mechanism by which SUN2 may be impacting HSV-1, we evaluated the spacing between the two nuclear membranes (Fig. 9). In line with a previous report by Mettenleiter and colleagues (36), overexpression of GFP-luSUN1 in RK13 cells led to a statistically significant separation of the two nuclear membranes from an average of 23.46 nm (control RK13) to 37.84 nm (RK13 GFP-luSUN1), a 60% increase. Interestingly, disrupting SUN2 had an even greater impact on the perinuclear space (42.49 nm for
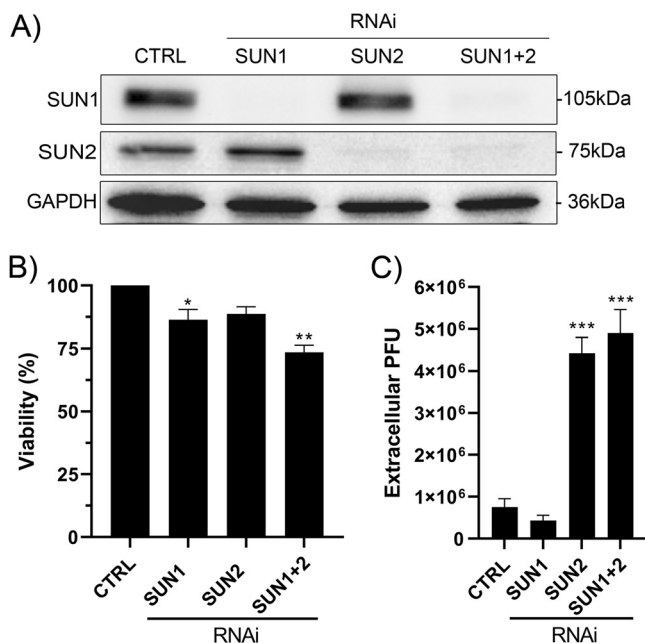
FIG 8 Knockdown of endogenous SUN2 by RNA interference promotes viral propagation in 143B cells. (A) Wild-type 143B cells were treated for 72 h with nonspecific RNAi (CRTL) or targeting SUN1, SUN2, or both. Levels of SUN proteins were then measured by Western blot. The proteins of interest were detected with specific SUN1 or SUN 2 antibodies and anti-GAPDH antibody was used as loading control (representative image among three independent experiments). (B) Viability of the treated cells was assessed by an alamarBlue assay. After the 72-h treatment with RNAi, 10% alamarBlue was added in the media for 3 h and then fluorescence measured ($n = 3$). (C) After treatment as in panel A, 143B cells were infected with HSV-1 at an MOI of 2 for 24 h. The supernatants were collected and titrated into Vero cells ($n = 3$). The error bars represent the SEM in all panels. Statistical analyses were done by one-way ANOVA with Dunnett multiple comparisons (*, $P \leq 0.05$; **, $P \leq 0.01$; ***, $P \leq 0.001$).

RK13 GFP-luSUN2, an 81% increase). We next measured the perinuclear spacing in the RNAi-treated 143B cells to determine if the RNAi reagents led to a similar outcome. As shown in Fig. 10, the perinuclear space was, on average, 29.96 nm in 143B cells (uninfected CTRL; gray violin). Inhibition of SUN1 modestly but statistically increased that space to 37.28 nm (25% increase). Disruption of SUN2 or both SUN1 and SUN2 led to similar values (38.28 nm or a 28% increase for SUN2 and 39.71 nm or a 33% increase for both proteins). In these uninfected cells, the impact of downregulating SUN1 or SUN2 on the perinuclear space was statistically undistinguishable. This indicated that both RNAi reagents worked as anticipated and altered the perinuclear space.

To probe if the virus could itself disrupt LINC complex, we next monitored the perinuclear space in the course of an infection. Interestingly, the data showed a modest but significant impact in infected 143B cells with a 17% increase of the perinuclear space to 35.10 nm (compare gray and red violin plots). In infected cells, knocking down SUN1 increased the spacing to 41.53 nm (50% increase) and knocking down SUN2 had a greater impact (50.02 nm or 67% increase), with a potentially concomitant effect when both proteins were knocked down (55.29 nm or an 84% increase). In infected cells, the impact on perinuclear spacing was statistically greatest when both SUN proteins were targeted, with SUN2 being the most impactful (Fig. 10). This confirmed once again that the RNAi reagents were functionally active. To finally determine how altering the LINC components is favorable for the virus, we monitored viral egress by electron microscopy in 143B cells preincubated with RNAi targeting SUN1, SUN2, or both. Under all conditions, viral particles were noted in the nucleus, cytoplasm, and cell surface (Fig. 11). Quantification of these particles indicates that the total number of viral particles per cell was not significantly impacted by the RNAi reagents, indicating that viral particle production was normal (Table 1). Similarly, knocking down SUN1 alone had no significant impact on viral distribution throughout the cell, with values
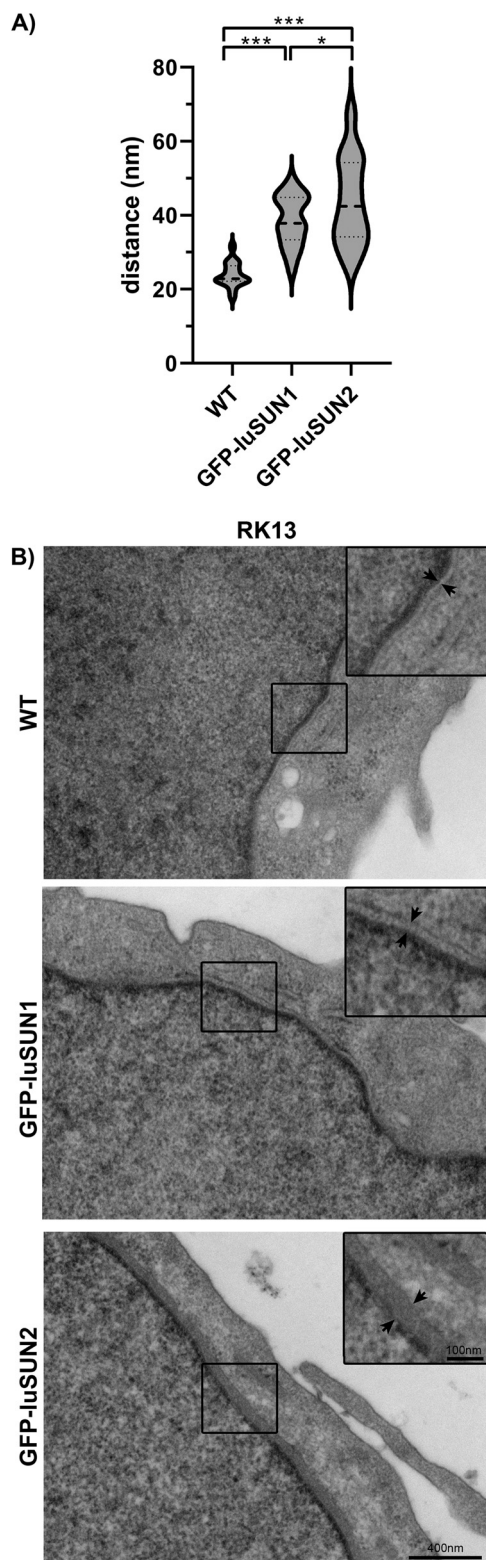
FIG 9 Overexpression of dominant negative forms of SUN1 or SUN2 in RK13 cell lines perturbs the spacing between the two nuclear membranes. Freshly sorted RK13 cell lines were grown to 90% confluence, fixed, and prepared for electron microscopy as detailed in Materials and Methods. (A) The distance between the inner and outer nuclear membranes, shown in violin plots, were measured at 5 to 15 places around the nucleus for each of 30 different cells per condition. The average distance between the membranes of each cell was considered a single data point. The median and 25% and 75% quartiles are shown. Statistical analyses were done by one-way ANOVA with Dunnett multiple comparisons (*, $P \leq 0.05$; ***, $P \leq 0.001$; $n = 30$). (B) Representative images. Outer and inner membranes are delineated with arrows in the zoomed images.
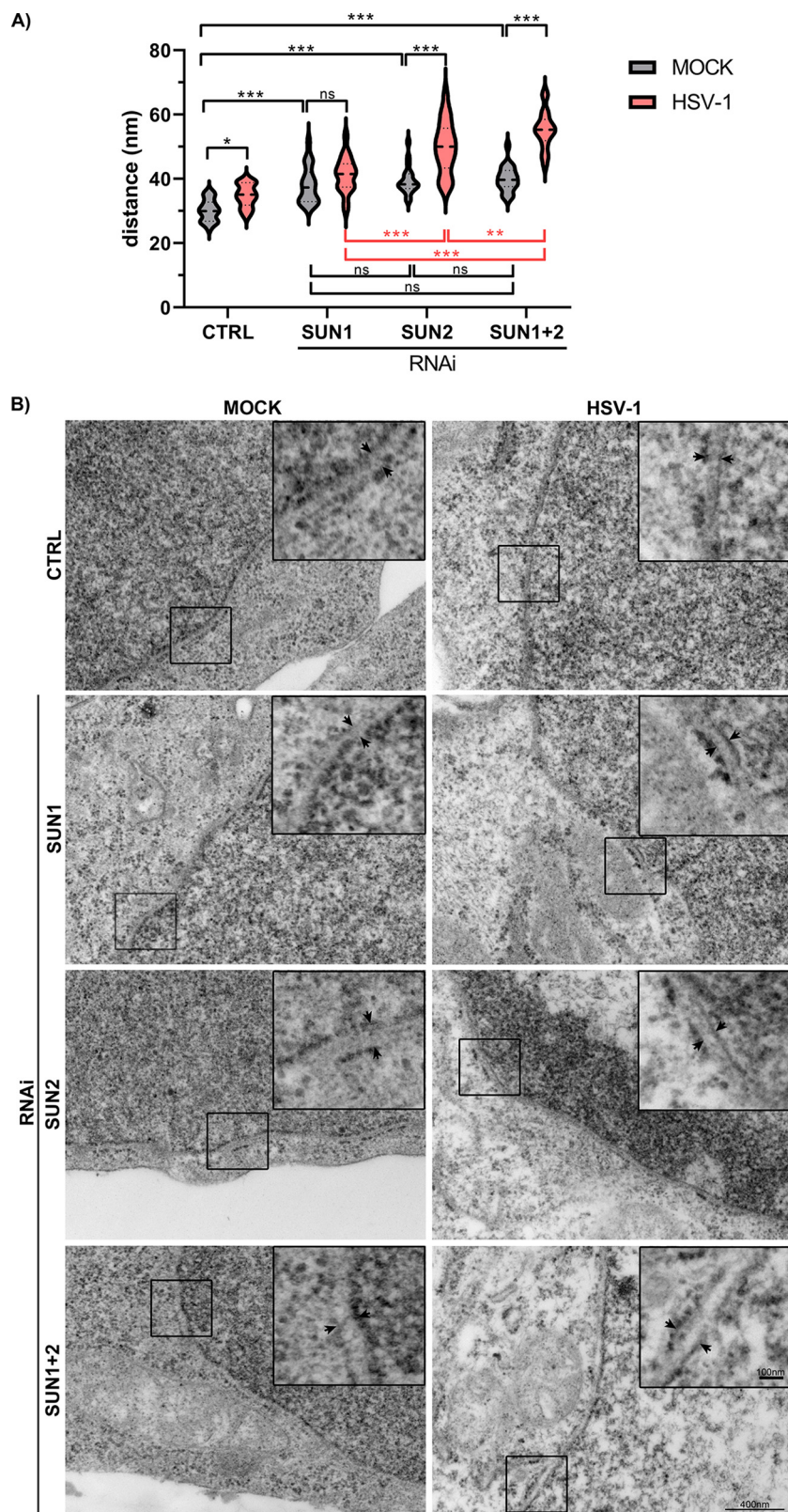
FIG 10 Inhibition of SUN1 or SUN2 by RNAi in 143B also perturbs the spacing between the two nuclear membranes. 143B cells were treated with RNAi for 72 h, mock treated, or infected with HSV-1 at an MOI of 2 for 12 h. Cells were then fixed and prepared for electron microscopy as detailed in Materials and Methods. (A) Distance between the two nuclear membranes were measured in 20 different cells per condition as in Fig. 9. The median and the 25% and 75% quartiles are indicated in the violin plots. Statistical analyses were done by one-way ANOVA with Dunnett multiple comparisons (ns: not significant; *, $P < 0.05$; **, $P < 0.01$; ***, $P < 0.001$; $n = 20$). (B) Representative images with zoom. Arrows indicate the position of the two nuclear membranes.
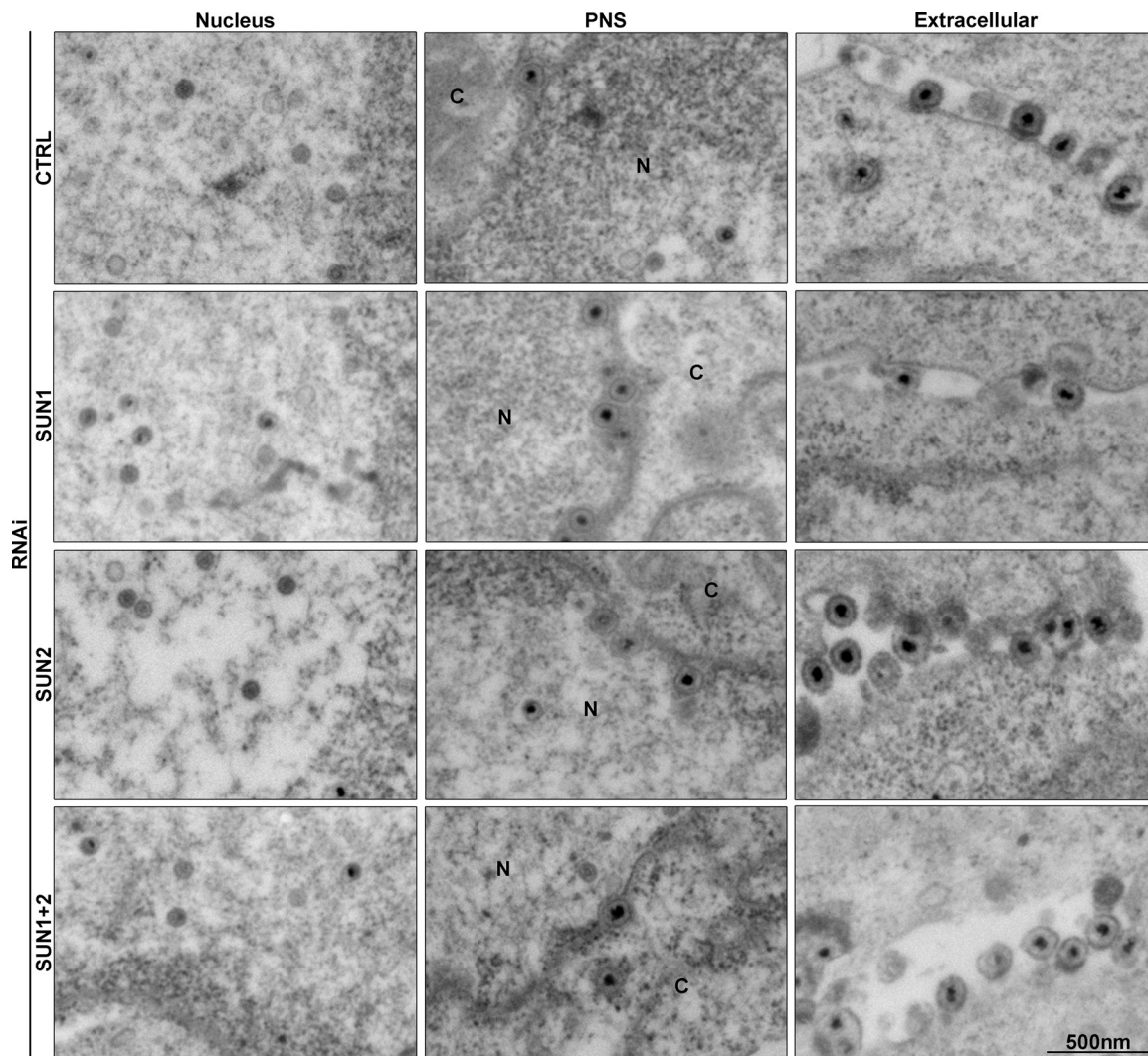
FIG 11 EM analysis of viral egress in SUN-depleted cells. 143B cells were treated with SUN1, SUN2, or nontargeting RNAi as described in Materials and Methods. At 72 h posttreatment, the cells were infected for 12 h with HSV-1 at an MOI of 2 and then fixed and processed for electron microscopy. N, nucleus; C, cytoplasm.

similar to those found for untreated cells. In contrast, knocking down SUN2 appeared to reduce the levels of nuclear capsids with a potential bias toward A-nuclear capsids. This reduction was similar to that observed when both SUN1 and SUN2 were targeted, confirming the implication of SUN2 over SUN1 in HSV-1 propagation. This decrease was matched with a higher number of viral particles at the extracellular membrane but oddly only when both SUN1 and SUN2 were targeted. It should be noted that these extracellular virions are those found at the plasma membrane, whereas plaque assays monitor virions released into the media. Taken together, this indicated that SUN2 has an antiviral effect as perturbing it stimulates viral egress without impacting viral particle assembly, presumably through its ability to modulate perinuclear spacing.

DISCUSSION

The formation of the LINC complex between SUN (INM) and KASH proteins (ONM) is critical to the tightly regulated spacing of the two nuclear envelopes. However, the egress of herpesviruses through the two nuclear membranes implies an increase of the perinuclear spacing to make room for the larger viral particles. That HCMV induces the measurable separation of the two nuclear membranes by reducing the expression level of both SUN1 and SUN2 is consistent with that scenario (35). In contrast,

TABLE 1 SUN inhibition promotes HSV-1 egress[a]

| Particle type | CTRL | RNAi[b] | | |
		SUN1	SUN2	SUN1 + SUN2
Nucleus				
A-capsids	29.2 ± 5.3 (15.7)	25.2 ± 4.8 (14.2)	**15.4 ± 2.2*** (10.2)*	17.1 ± 2.5 (7.9)*
B-capsids	75.1 ± 18.5 (40.4)	59.5 ± 10.0 (33.6)	54.0 ± 9.3 (35.9)	54.5 ± 9.4 (25.2)
C-capsids	23.0 ± 3.4 (12.4)	19.1 ± 2.3 (10.8)	21.0 ± 2.4 (14.0)	23.3 ± 3.3 (10.8)
Total	127.2 ± 25.3 (68.5)	103.8 ± 15.4 (58.6)	90.4 ± 10.0 (60.1)	**94.9 ± 12.8*** (43.9)*
PNS	10.0 ± 2.0 (5.4)	15.6 ± 4.5 (8.8)	10.1 ± 1.8 (6.8)	13.9 ± 3.6 (6.5)
Cytoplasm	35.2 ± 8.3 (18.9)	43.8 ± 8.4 (24.7)	34.0 ± 7.0 (22.6)	64.4 ± 18.4 (29.7)
Extracellular	13.4 ± 3.6 (7.3)	14.0 ± 3.0 (8.0)	16.1 ± 3.2 (10.7)	**42.8 ± 7.2***** (19.8)**
Total	185.8 ± 23.8 (100)	177.1 ± 19.1 (100)	150.5 ± 10.4 (100)	216.0 ± 25.4 (100)

[a]Average number of viral particles per cell and SEM ($n = 20$). The value in parentheses indicates the percentage of the total particles/cell.
[b]Statistical analyses were done by one-way ANOVA as before (*, $P < 0.05$; **, $P < 0.01$; ***, $P < 0.001$), testing the average number of viral particles (bold values) or the percentage.

inactivation of SUN2 by overexpression of a dominant negative mutant surprisingly impairs the propagation of PrV, albeit it is not clear if cell-associated virions or those released in the media were quantified (36). To further address the role of LINC in the dissemination of herpesviruses, we therefore probed its implication on HSV-1. We disrupted it by two different and orthogonal approaches, namely, by overexpression of the dominant negative luminal portion of SUN1 or SUN2 or with RNAi targeting these proteins. The data revealed that disrupting SUN2 by overexpressing the luminal portion of the protein, but not that of SUN1, favors the propagation of HSV-1 in RK13 cells. RNA interference targeting endogenous SUN2 in 143B cells, which was very efficient (93%), led to significantly increased HSV-1 yields, indicating that functional SUN2 normally impedes HSV-1 yields in these two different cell lines. Electron microscopy data indicated that this phenomenon was independent of viral particle assembly and rather depended on their egress toward the cell periphery. Given that the luminal portion of SUN2 has a similar outcome as inhibiting SUN2 altogether, a possible scenario is that SUN2 inhibition promotes nuclear viral egress by separating the two nuclear membranes. However, this scenario remains to be formally validated.

It is interesting to note that inactivation of SUN1 did not have any appreciable effect on HSV-1 propagation. This was unlikely due to a better inhibition of SUN2, since both SUN1 and SUN2 protein levels were efficiently knocked down by RNA interference and only SUN2 disruption had a phenotype in RK13 cells. Why this is the case is up to speculation. Though we showed that the dominant constructs and RNAi reagents were functional and led to an increased perinuclear space, SUN2 appears to have a preponderant impact on both the perinuclear space and viral egress. It is therefore possible that SUN1 disruption does not sufficiently distance the two nuclear membranes to accommodate the large viral particles or perhaps that SUN1 is not present at the specific sites of viral nuclear egress. Although SUN1 and SUN2 have largely redundant roles, small differences in their functions or interaction partners may also be an important factor (54–56). For example, it has previously been reported that SUN2, but not SUN1, is indispensable for anchoring mini-Nesprin 2G, a chimeric form of Nesprin-2, to the outer nuclear membrane (57), but any link with HSV-1 has yet to be uncovered. Similarly, SUN2, but not SUN1, interacts with TMEM43 and Rab5 (58, 59). Rab5 is a component of mature HSV-1 virions (40, 60) that is typically implicated in endocytic processes, vesicular transport, and signaling (61). Rab5 has also been implicated in HSV-1 egress downstream of the nucleus (62), opening up the possibility that SUN2 may act elsewhere than at the nuclear level. Meanwhile, TMEM43, which is involved in maintaining the integrity of the nuclear envelope (59), has been detected as an interaction partner of the HSV-1 glycoprotein M, but its role in the HSV-1 cycle remains undefined (63). Perhaps most interesting is TorsinA, which modulates the nuclear localization of SUN2 but not SUN1 (64) and favors HSV-1 and PrV nuclear egress

TABLE 2 Gibson assembly primers

Gene	Forward primer (5′ → 3′)	Reverse primer (5′ → 3′)
GFP-luSUN1	GTGAACCGTCAGATCGCCTGGAGAATTGGCTAGCGGATCCATGCTGCTATCCGTGCCGTT	TACAGTCGACTCTAGAATTCTGCAGTTAACCGGTGGATCCTCACAGTTCGTCCTTGCTAG
GFP-luSUN2	GTGAACCGTCAGATCGCCTGGAGAATTGGCTAGCGGATCCATGTGCTATCCGTGCCGTT	TACAGTCGACTCTAGAATTCTGCAGTTAACCGGTGGATCCTCACAGTTCGTCCTTGCTAG

(15, 65). How the virus functionally interacts with TorsinA and SUN2 certainly warrants further research.

In the present study, we experimentally altered LINC components and monitored HSV-1 propagation. However, given that the virus makes its way through the tight perinuclear space, one can presume that the virus can modulate it on its own, a scenario that is supported by the present study. However, the molecular details of such action have yet to be uncovered. One mechanism, mentioned above, is to restrict the level of expression of LINC components as HCMV does (34). Though not formally ruled out, that HSV-1 did not hamper SUN expression in the inducible 143B cell lines or in the constitutively expressing RK13 cells suggests that this is perhaps not the case. Other possible scenarios are that the virus laterally displaces the LINC complexes to open up a sufficiently large space or that the virus somehow breaks up the LINC complexes and dissociates SUN from KASH, "unzipping" the two nuclear membranes in either case. While the present data imply that spacing between the two nuclear membranes limits HSV-1 egress, it is also conceivable that SUN2 acts independently of its interaction with KASH proteins, as reported for HIV where SUN2 expression levels modulate the antiviral protein cyclophilin A (66, 67). It would thus be interesting to know if a similar mechanism justifies the seemingly opposite effects of SUN2 on PrV and HSV-1, perhaps though distinct SUN2 interacting partners. Alternative SUN2 isoforms, which exist in three varieties (https://www.uniprot.org/), may also contribute to this differential effect on the egress of the two viruses. Elucidating how herpesviruses manipulate LINC at the molecular level will thus be most interesting.

MATERIALS AND METHODS

Plasmids. pGFP-luSUN1 and pGFP-luSUN2 are pcDNA3.1-based plasmids provided courtesy of Thomas Mettenleiter's laboratory (Friedrich-Loeffler-Institut, Greifswald, Germany) (36). Both express the luminal portion of SUN1 or SUN2 (i.e., found in the perinuclear space) preceded by GFP at their amino terminus. Upon reception, *Escherichia coli* strain DH5α was transformed, the plasmids isolated with NucleoBond Xtra midikits (Macherey-Nagel), and sequenced, which confirmed the absence of undesired mutations. pMD2-pRRE, pRSV-REV, and pMD2-VSVg plasmids are a third-generation lentiviral packaging system (68, 69). The plasmid pCW-MCS provided puromycin resistance and a TET-ON type TREtight promoter (70) that can be induced by the tetracycline doxycycline (71). These plasmids were used for the generation of inducible 143B cell lines as described below.

143B cell lines. The human osteosarcoma 143B thymidine kinase-negative cell line was maintained in culture in Dulbecco modified Eagle medium (DMEM) supplemented with 5% bovine growth serum (BGS), 1% L-glutamine, and 15 μg/mL 5-bromo-2-deoxyuridine (BUdR) (Sigma-Aldrich). Prior to transfections and infections, cells were maintained in DMEM without BUdR for 24 h. Inducible 143B cell lines were produced by transducing them with lentiviruses coding either for GFP-luSUN1 or GFP-luSUN2. These genes were initially subcloned into the inducible plasmid pCW-MCS using Gibson's assembly (72). To this end, GFP-luSUN1 and GFP-luSUN2 were PCR amplified from the plasmids pGFP-luSUN1 and pGFP-luSUN2 described above using the primers specified in Table 2. The plasmid pCW-MCS was linearized using the restriction enzyme DPN-1 and mixed with either PCR product at a molar ratio of 1:3 (plasmid/PCR) and 2× Gibson reagent (10% PEG-8000, 200 mM Tris-HCl pH 7.5, 20 mM MgCl$_2$, 20 mM dithiothreitol [DTT], 0.4 mM [each] of the four deoxynucleoside triphosphates [dNTPs], 2 mM NAD, 10 U/μL T5 exonuclease [NEB no. M0363S], 2 U/μL Phusion [NEB no. M0530S], 40 U/μL *Taq* Ligase [NEB no. M0208S]) as previously described (72). Following an incubation at 50°C for 1 h, the reaction was diluted 1:5, and 5 μL was added to 50 μL of chemically competent *E. coli* JM109 cells. Positive colonies were grown overnight at 37°C with agitation and plasmids extracted using the NucleoBond midiprep kit according to the manufacturer's instructions. To package the inducible plasmids in lentiviruses, HEK 293T/17 (ATCC CRL-11268) cells were seeded into a six-well plate 1 day prior to transfection. On the following day, 1.25 μg pCW-MCS-GFP-luSUN1, pCW-MCS-GFP-luSUN2, or pHAGE-mCherry as a transduction control was mixed with 0.3125 μg pMD2-pRRE, 0.3125 μg pRSV-REV, and 0.625 μg pMD2-VSVg in 200 μL of RPMI. The plasmid solution was mixed, and 7.5 μL of TransIT (Mirus Bio) was added. The transfection mixture was incubated at room temperature for 20 min and then added dropwise to the cells,

which were then maintained at 37°C overnight. Subsequently, the supernatant was replaced with 4.5 mL DMEM (Wisent Bioproducts) supplemented with 15% fetal bovine serum (FBS) and 25 mM HEPES. Within 36 h, the lentiviruses contained in the supernatant were harvested and used immediately for transduction of 143B cells (human osteosarcoma, thymidine kinase-negative; ATCC CRL-8303) (69). The collected virus was first centrifuged at 2,000 $\times$ g for 5 min and then filtered using a syringe filter (0.45 μm; SFCA) to remove large cell debris. For transduction of 143B cells, viral supernatant (1 mL) was added to subconfluent cells grown in a 6-well plate in the presence of 10 μg/mL of Polybrene and incubated overnight. The following day, the culture medium was replaced with fresh medium, and the cells were incubated for an additional 24 h before passaging. The cells were then expanded in culture for 1 week and submitted to puromycin selection (0.5 μg/mL). Cells were finally incubated overnight with 1 μg/mL doxycycline (DOX) to induce GFP-tagged protein expression and sorted with FACS Aria (BD).

RK13 cell lines. Wild-type RK13 (rabbit kidney, ATCC CCL-37) or expressing GFP-luSUN1 (RK13 GFP-luSUN1) or SUN2 (RK13 GFP-luSUN2) were kindly donated by Thomas Mettenleiter's laboratory (36). On reception, these cell lines were maintained in culture in modified Eagle essential medium (EMEM) (Wisent Bioproducts) supplemented with 5% bovine growth serum (BGS), 1% L-glutamine, and, in the case of the transfected cells, 500 μg/mL G418. Cells were maintained at 37°C with 5% CO_2, passed at 90% confluence and tested for contaminating mycoplasma. GFP-positive RK13 GFP-luSUN1 and SUN2 cell lines were additionally sorted by FACS, maintained in culture, and then reanalyzed by FACS, Western blotting, and immunofluorescence as detailed in the results section.

Antibodies. Primary antibodies for Western blotting (WB) and immunofluorescence (IF) were commercially purchased from the following sources: monoclonal anti-GFP (WB, 1:1,000; Sigma; 11-814-460-001), monoclonal anti-gamma tubulin (WB, 1:10,000; Sigma; T6557), monoclonal anti-ICP4 (IF, 1:200; Abcam; ab6514), monoclonal anti-glyceraldehyde-3-phosphate dehydrogenase (GAPDH) (WB, 1:5,000; Millipore Sigma; MAB374), monoclonal anti-SUN1 (WB, 1:5,000; Abcam; 124770), polyclonal anti-SUN1 (WB, 1:1,000; Sigma-Aldrich; HPA008346 targeting amino acid 470 to 600 contained in the endogenous SUN1 only), and polyclonal anti-SUN2 (WB, 1:1,000; Sigma-Aldrich HPA001209 targeting amino acid 390 to 540 contained in the endogenous SUN2 and exogenous GFP-luSUN2). All secondary antibodies for IF were ordered from Molecular Probes and those for WB from Jackson ImmunoResearch.

RNA interference. Wild-type (i.e., non-lentivirus transduced) 143B cells were seeded in 6-well plates 24 h prior to transfection in BUdR-free medium. Cells were transfected for 72 h with the transfection agent LipoJet (SignaGen Laboratories; SL100468) according to the manufacturer's instructions. Upon screening of various RNAi reagents and concentrations for their efficacy by Western blotting, we opted for 100 nM nonspecific Dicer-substrate small interfering RNA (dsiRNA) (dsiCTL; IDT; DS NC1) as control, 25 nM siRNA against SUN1 (Dharmacon), and 100 nM dsiRNA against SUN2 (IDT).

Cell viability. Cell viability was assessed with the alamarBlue assay (Bio-Rad). Briefly, 143B cells grown in 96-well plates were treated with the RNAi for 72 h. AlamarBlue was added to the cells to a final concentration of 10% for 3 h at 37°C before cell viability was measured using a ClarioStar microplate reader (BMG Labtech; software version 5.20 R5). The percentages of cell viability were normalized with the control RNAi condition.

Virus and infections. 143B or RK13 cells were grown in 6-well plates for 24 h at 37°C with 5% CO_2. For immunofluorescence analyses, the cells were instead seeded in 6-well plates with three coverslips (Fisherbrand) per well. Inducible 143B lines were treated or not with DOX at a concentration of 1 μg/mL at the time of plating. Cells were then mock treated or infected with HSV-1 (HSV-1 17+ wild-type virus provided by Beate Sodeik) at a multiplicity of infection (MOI) of 2 and then complemented with fresh medium and incubated at 37°C for 9 h for the RK13 and 12 h for 143B cells. Where indicated, the cells were analyzed by FACS or the virus released in the tissue culture milieu collected and spun at 500 $\times$ g for 5 min to remove aggregates. These viruses were then stored at -80°C until their titrations on Vero cells as detailed below.

Plaque assays. Twenty-four hours prior to titration, Vero cells (ATCC CCL-81) were seeded in 6-well plates to obtain a monolayer of confluent cells. Supernatants from the above infections were serially diluted in RPMI-0.1% bovine serum albumin (BSA) and added to the Vero cell monolayer. One hour later, 2$\times$ DMEM (10% BGS, 2% penicillin/streptomycin, 2% L-glutamine) mixed with 2% agarose in a 1:1 ratio was added to the infected monolayer. The infected cells were incubated at 37°C for 3 days before the DMEM agarose medium was removed from the monolayer and the cells fixed with -20°C cold 100% methanol. The methanol was removed, and a 0.1% crystal violet solution was then added to the fixed cells for staining. Taking into account the dilution and the volume used, the initial viral titer was calculated using the number of PFU produced by the virus in each sample.

FACS sorting and analysis. 143B inducible cell lines were induced or not with DOX at a concentration of 1 μg/mL for 24 h. Inducible 143B cell lines, or RK13 cell lines, were washed twice with cold phosphate-buffered saline (PBS), trypsinized, and centrifuged at 500 $\times$ g for 5 min at 4°C. For sorting, the cell pellet was washed twice with cold PBS and resuspended in sorting buffer (0.2-μm filtered 1$\times$ PBS, 1 mM EDTA, 25 mM HEPES pH 7.0, 1% FBS). GFP-positive cells were collected at the cytometry platform of the CHU Sainte-Justine Research Centre (CHUSJRC) or the Department of Microbiology, Immunology, and Infectiology of the Université de Montréal and used immediately or recultured.

For FACS analyses, the cell pellet was washed twice with ice-cold PBS and resuspended in PBS-1% FBS. Data collection was performed in Canto II FACS or Fortessa LSR at the CHUSJRC cytometry platform, and data were analyzed with FlowJo software version 10.6.1. The graphs (see results) show the fluorescence intensity on the x axes, and the percentage of cells with the corresponding intensity on the y axes.

Immunofluorescence. 143B or RK13 cells seeded on slides were fixed with 3% paraformaldehyde for 20 min at 4°C and permeabilized with 0.1% triton for 4 min at room temperature. The slides were subsequently incubated at room temperature for 30 min in a blocking solution containing 10% fetal calf serum (FCS) in PBS to block nonspecific binding and then incubated for 1 h with the primary antibody

(anti-ICP4; 1:200) diluted in the same blocking solution. After three washes with PBS, the cells were incubated for 45 min with the secondary antibody, goat anti-mouse Alexa 568 (1:1,000) diluted in PBS. The slides were assembled with Dako (Dako) containing 10 μg/mL Hoechst 33342 (Sigma-Aldrich) overnight on a microscope slide. Images of the cells were captured with a confocal laser scanning microscope (Leica TCS SP8) from the CHUSJRC microscopy platform and analyzed with LAS X software version 3.7.0.20979.

Western blotting. 143B or RK13 cells were collected with radioimmunoprecipitation assay (RIPA) buffer (20% SDS, 1% NP-40, 1% deoxycholic acid, 150 mM NaCl, 10 mM Tris-HCl pH 7.4, freshly supplemented with a cocktail of protease inhibitors). Sample concentrations were quantified using the Pierce bicinchoninic acid (BCA) protein assay kit (Thermo Fisher Scientific) and measured with a ClarioStar plate reader from the CHUSJRC's molecular biology platform. Samples were separated on 5 to 20% SDS-PAGE gradient gels and proteins then transferred to a polyvinylidene difluoride (PVDF) membrane (Bio-Rad). The membranes were blocked for 1 h at room temperature in a 5% milk solution in Tris-buffered saline-Tween 20 (TBST) (13.7 mM NaCl, 0.27 mM KCl, 0.2 mM KH$_2$PO$_4$, 1 mM Na$_2$HPO$_4$, 0.1% Tween 20). Primary antibody diluted in 5% BSA-TBST was added to the membrane for an overnight incubation at 4°C. Membranes were then washed three times for 5 min with TBST and incubated for 1 h at room temperature (RT) with the appropriate secondary antibodies conjugated to horseradish peroxidase diluted in 5% milk TBST. Proteins were revealed using the ChemiDoc (Bio-Rad) system after addition of the enhanced chemiluminescence (ECL) (Bio-Rad) substrate.

Electron microscopy. 143B WT and RK13 cells were seeded in 6-well plates. 143B WT cells were transfected with RNAi reagents targeting SUN1 or SUN2 for 72 h and then infected for 12 h. Next, both cell types were fixed in a solution of 2.5% glutaraldehyde and 2% paraformaldehyde in 0.1 M cacodylate buffer pH 7.2 overnight and then stored in fresh cacodylate buffer. Cells were next resuspended in 0.1% osmium tetroxide prepared in cacodylate buffer at 4°C for an hour and gradually dehydrated with ethanol. Finally, cells were treated with propylene oxide for permeabilization and embedded on Epon. Samples were then cut with a Leica (MZ6) Ultracut UCT ultramicrotome and analyzed with a Philips Tecnai 12 transmission electron microscope from the Electron Microscopy Facility of the Université de Montréal. To analyze the distance between nuclear membranes, between 5 to 15 measures were taken for each cell for 20 to 30 cells per condition. The average measures for a given cell were considered single data points. Alternatively, to quantify viral egress, all viral particles were counted in 20 cells per condition from two independent experiments (i.e., 3,000 to 4,300 viral particles per condition). Table 1 shows the average number of particles per cell along with the standard errors of the mean (SEM). Numbers in parentheses reflect the proportion of all particles in the cell (%). Statistics were done both on average particles and on normalized percentages.

Statistics. One-way analysis of variance (ANOVA) with Dunnett multiple comparisons were used to determine the significance of the data using GraphPad Prism software version 8.2.1. The difference between the control conditions and the experimental conditions was considered statistically significant when the P value was less than 0.05.

REFERENCES

1. Petti S, Lodi G. 2019. The controversial natural history of oral herpes simplex virus type 1 infection. Oral Dis 25:1850–1865. https://doi.org/10.1111/odi.13234.

2. Tabbara KF, Al Balushi N. 2010. Topical ganciclovir in the treatment of acute herpetic keratitis. Clin Ophthalmol 4:905–912. https://doi.org/10.2147/opth.s8666.

3. Whitley R, Baines J. 2018. Clinical management of herpes simplex virus infections: past, present, and future. F1000Res 7:1726. https://doi.org/10.12688/f1000research.16157.1.

4. Johnson DC, Baines JD. 2011. Herpesviruses remodel host membranes for virus egress. Nat Rev Microbiol 9:382–394. https://doi.org/10.1038/nrmicro2559.

5. Crump C. 2018. Virus assembly and egress of HSV. Adv Exp Med Biol 1045:23–44. https://doi.org/10.1007/978-981-10-7230-7_2.

6. Miranda-Saksena M, Boadle RA, Aggarwal A, Tijono B, Rixon FJ, Diefenbach RJ, Cunningham AL. 2009. Herpes simplex virus utilizes the large secretory vesicle pathway for anterograde transport of tegument and envelope proteins and for viral exocytosis from growth cones of human fetal axons. J Virol 83:3187–3199. https://doi.org/10.1128/JVI.01579-08.

7. Lippe R. 2020. Intracellular transport of Alphaherpesvirinae. Virologie (Montrouge) 24:210–230. https://doi.org/10.1684/vir.2020.0851.

8. Roller RJ, Zhou Y, Schnetzer R, Ferguson J, DeSalvo D. 2000. Herpes simplex virus type 1 U(L)34 gene product is required for viral envelopment. J Virol 74:117–129. https://doi.org/10.1128/jvi.74.1.117-129.2000.

9. Reynolds AE, Ryckman BJ, Baines JD, Zhou Y, Liang L, Roller RJ. 2001. U(L)31 and U(L)34 proteins of herpes simplex virus type 1 form a complex that accumulates at the nuclear rim and is required for envelopment of nucleocapsids. J Virol 75:8803–8817. https://doi.org/10.1128/jvi.75.18.8803-8817.2001.

10. Fuchs W, Klupp BG, Granzow H, Osterrieder N, Mettenleiter TC. 2002. The interacting UL31 and UL34 gene products of pseudorabies virus are involved in egress from the host-cell nucleus and represent components of primary enveloped but not mature virions. J Virol 76:364–378. https://doi.org/10.1128/jvi.76.1.364-378.2002.

11. Reynolds AE, Wills EG, Roller RJ, Ryckman BJ, Baines JD. 2002. Ultrastructural localization of the herpes simplex virus type 1 UL31, UL34, and US3 proteins suggests specific roles in primary envelopment and egress of nucleocapsids. J Virol 76:8939–8952. https://doi.org/10.1128/jvi.76.17.8939-8952.2002.

12. Bjerke SL, Roller RJ. 2006. Roles for herpes simplex virus type 1 UL34 and US3 proteins in disrupting the nuclear lamina during herpes simplex virus type 1 egress. Virology 347:261–276. https://doi.org/10.1016/j.virol.2005.11.053.

13. Simpson-Holley M, Colgrove RC, Nalepa G, Harper JW, Knipe DM. 2005. Identification and functional evaluation of cellular and viral factors involved in the alteration of nuclear architecture during herpes simplex virus 1 infection. J Virol 79:12840–12851. https://doi.org/10.1128/JVI.79.20.12840-12851.2005.

14. Kato A, Oda S, Watanabe M, Oyama M, Kozuka-Hata H, Koyanagi N, Maruzuru Y, Arii J, Kawaguchi Y. 2018. Roles of the phosphorylation of herpes simplex virus 1 UL51 at a specific site in viral replication and pathogenicity. J Virol 92:e01035-18. https://doi.org/10.1128/JVI.01035-18.

15. Maric M, Shao J, Ryan RJ, Wong CS, Gonzalez-Alegre P, Roller RJ. 2011. A functional role for TorsinA in herpes simplex virus 1 nuclear egress. J Virol 85:9667–9679. https://doi.org/10.1128/JVI.05314-11.

16. Park R, Baines JD. 2006. Herpes simplex virus type 1 infection induces activation and recruitment of protein kinase C to the nuclear membrane and increased phosphorylation of lamin B. J Virol 80:494–504. https://doi.org/10.1128/JVI.80.1.494-504.2006.

17. Liu Z, Kato A, Oyama M, Kozuka-Hata H, Arii J, Kawaguchi Y. 2015. Role of host cell p32 in herpes simplex virus 1 de-envelopment during viral nuclear egress. J Virol 89:8982–8998. https://doi.org/10.1128/JVI.01220-15.

18. Roussel E, Lippe R. 2018. Cellular protein kinase D modulators play a role during multiple steps of herpes simplex virus 1 egress. J Virol 92:e01486-18. https://doi.org/10.1128/JVI.01486-18.

19. Sosa BA, Kutay U, Schwartz TU. 2013. Structural insights into LINC complexes. Curr Opin Struct Biol 23:285–291. https://doi.org/10.1016/j.sbi.2013.03.005.

20. Rothballer A, Schwartz TU, Kutay U. 2013. LINCing complex functions at the nuclear envelope: what the molecular architecture of the LINC complex can reveal about its function. Nucleus 4:29–36. https://doi.org/10.4161/nucl.23387.

21. Starr DA, Fridolfsson HN. 2010. Interactions between nuclei and the cytoskeleton are mediated by SUN-KASH nuclear-envelope bridges. Annu Rev Cell Dev Biol 26:421–444. https://doi.org/10.1146/annurev-cellbio-100109-104037.

22. Darlington RW, Moss LH, III. 1968. Herpesvirus envelopment. J Virol 2:48–55. https://doi.org/10.1128/JVI.2.1.48-55.1968.

23. Nii S, Morgan C, Rose HM. 1968. Electron microscopy of herpes simplex virus. II. Sequence of development. J Virol 2:517–536. https://doi.org/10.1128/JVI.2.5.517-536.1968.

24. Stackpole CW. 1969. Herpes-type virus of the frog renal adenocarcinoma. I. Virus development in tumor transplants maintained at low temperature. J Virol 4:75–93. https://doi.org/10.1128/JVI.4.1.75-93.1969.

25. Granzow H, Klupp BG, Fuchs W, Veits J, Osterrieder N, Mettenleiter TC. 2001. Egress of alphaherpesviruses: comparative ultrastructural study. J Virol 75:3675–3684. https://doi.org/10.1128/JVI.75.8.3675-3684.2001.

26. Remillard-Labrosse G, Guay G, Lippé R. 2006. Reconstitution of herpes simplex virus type 1 nuclear capsid egress in vitro. J Virol 80:9741–9753. https://doi.org/10.1128/JVI.00061-06.

27. Crisp M, Liu Q, Roux K, Rattner JB, Shanahan C, Burke B, Stahl PD, Hodzic D. 2006. Coupling of the nucleus and cytoplasm: role of the LINC complex. J Cell Biol 172:41–53. https://doi.org/10.1083/jcb.200509124.

28. Starr DA. 2011. KASH and SUN proteins. Curr Biol 21:R414–R415. https://doi.org/10.1016/j.cub.2011.04.022.

29. Meinke P, Schirmer EC. 2015. LINC'ing form and function at the nuclear envelope. FEBS Lett 589:2514–2521. https://doi.org/10.1016/j.febslet.2015.06.011.

30. Cruz VE, Esra Demircioglu F, Schwartz TU. 2020. Structural analysis of different LINC complexes reveals distinct binding modes. J Mol Biol 432:6028–6041. https://doi.org/10.1016/j.jmb.2020.09.019.

31. Kozono T, Tadahira K, Okumura W, Itai N, Tamura-Nakano M, Dohi T, Tonozuka T, Nishikawa A. 2018. Jaw1/LRMP has a role in maintaining nuclear shape via interaction with SUN proteins. J Biochem 164:303–311. https://doi.org/10.1093/jb/mvy053.

32. Gundersen GG, Worman HJ. 2013. Nuclear positioning. Cell 152:1376–1389. https://doi.org/10.1016/j.cell.2013.02.031.

33. Jansen KA, Atherton P, Ballestrem C. 2017. Mechanotransduction at the cell-matrix interface. Semin Cell Dev Biol 71:75–83. https://doi.org/10.1016/j.semcdb.2017.07.027.

34. Bhargava A, Lahaye X, Manel N. 2018. Let me in: control of HIV nuclear entry at the nuclear envelope. Cytokine Growth Factor Rev 40:59–67. https://doi.org/10.1016/j.cytogfr.2018.02.006.

35. Buchkovich NJ, Maguire TG, Alwine JC. 2010. Role of the endoplasmic reticulum chaperone BiP, SUN domain proteins, and dynein in altering nuclear morphology during human cytomegalovirus infection. J Virol 84:7005–7017. https://doi.org/10.1128/JVI.00719-10.

36. Klupp BG, Hellberg T, Granzow H, Franzke K, Dominguez Gonzalez B, Goodchild RE, Mettenleiter TC. 2017. Integrity of the linker of nucleoskeleton and cytoskeleton is required for efficient herpesvirus nuclear egress. J Virol 91:e00330-17. https://doi.org/10.1128/JVI.00330-17.

37. Campadelli G, Brandimarti R, Di Lazzaro C, Ward PL, Roizman B, Torrisi MR. 1993. Fragmentation and dispersal of Golgi proteins and redistribution of glycoproteins and glycolipids processed through the Golgi apparatus after infection with herpes simplex virus 1. Proc Natl Acad Sci U S A 90:2798–2802. https://doi.org/10.1073/pnas.90.7.2798.

38. Turcotte S, Letellier J, Lippé R. 2005. Herpes simplex virus type 1 capsids transit by the trans-Golgi network, where viral glycoproteins accumulate independently of capsid egress. J Virol 79:8847–8860. https://doi.org/10.1128/JVI.79.14.8847-8860.2005.

39. Zhang J, Nagel CH, Sodeik B, Lippé R. 2009. Early, active, and specific localization of herpes simplex virus type 1 gM to nuclear membranes. J Virol 83:12984–12997. https://doi.org/10.1128/JVI.01180-09.

40. Stegen C, Yakova Y, Henaff D, Nadjar J, Duron J, Lippé R. 2013. Analysis of virion-incorporated host proteins required for herpes simplex virus type 1 infection through a RNA interference screen. PLoS One 8:e53276. https://doi.org/10.1371/journal.pone.0053276.

41. El Kasmi I, Lippé R. 2015. Herpes simplex virus 1 gN partners with gM to modulate the viral fusion machinery. J Virol 89:2313–2323. https://doi.org/10.1128/JVI.03041-14.

42. El Kasmi I, Khadivjam B, Lackman M, Duron J, Bonneil E, Thibault P, Lippé R. 2018. Extended synaptotagmin 1 interacts with herpes simplex virus 1 glycoprotein M and negatively modulates virus-induced membrane fusion. J Virol 92:e01281-17. https://doi.org/10.1128/JVI.01281-17.

43. Smiley JR. 2004. Herpes simplex virus virion host shutoff protein: immune evasion mediated by a viral RNase? J Virol 78:1063–1068. https://doi.org/10.1128/jvi.78.3.1063-1068.2004.

44. Birkenheuer CH, Danko CG, Baines JD. 2018. Herpes simplex virus 1 dramatically alters loading and positioning of RNA polymerase II on host genes early in infection. J Virol 92:e02184-17. https://doi.org/10.1128/JVI.02184-17.

45. Cui YH, Liu Q, Xu ZY, Li JH, Hu ZX, Li MJ, Zheng WL, Li ZJ, Pan HW. 2019. Quantitative proteomic analysis of human corneal epithelial cells infected with HSV-1. Exp Eye Res 185:107664. https://doi.org/10.1016/j.exer.2019.05.004.

46. Liu H, Huang CX, He Q, Li D, Luo MH, Zhao F, Lu W. 2019. Proteomics analysis of HSV-1-induced alterations in mouse brain microvascular endothelial cells. J Neurovirol 25:525–539. https://doi.org/10.1007/s13365-019-00752-z.

47. Wan W, Wang L, Chen X, Zhu S, Shang W, Xiao G, Zhang LK. 2019. A subcellular quantitative proteomic analysis of herpes simplex virus type 1-infected HEK 293T cells. Molecules 24:4215. https://doi.org/10.3390/molecules24234215.

48. Hensel N, Raker V, Förthmann B, Buch A, Sodeik B, Pich A, Claus P. 2020. The proteome and secretome of cortical brain cells infected with herpes simplex virus. Front Neurol 11:844. https://doi.org/10.3389/fneur.2020.00844.

49. Ouwendijk WJD, Dekker LJM, van den Ham HJ, Lenac Rovis T, Haefner ES, Jonjic S, Haas J, Luider TM, Verjans G. 2020. Analysis of virus and host proteomes during productive HSV-1 and VZV infection in human epithelial cells. Front Microbiol 11:1179. https://doi.org/10.3389/fmicb.2020.01179.

50. Soh TK, Davies CTR, Muenzner J, Hunter LM, Barrow HG, Connor V, Bouton CR, Smith C, Emmott E, Antrobus R, Graham SC, Weekes MP, Crump CM. 2020. Temporal proteomic analysis of herpes simplex virus 1 infection reveals cell-surface remodeling via pUL56-mediated GOPC degradation. Cell Rep 33:108235. https://doi.org/10.1016/j.celrep.2020.108235.

51. Hodzic DM, Yeater DB, Bengtsson L, Otto H, Stahl PD. 2004. Sun2 is a novel mammalian inner nuclear membrane protein. J Biol Chem 279:25805–25812. https://doi.org/10.1074/jbc.M313157200.

52. Lu W, Gotzmann J, Sironi L, Jaeger VM, Schneider M, Luke Y, Uhlen M, Szigyarto CA, Brachner A, Ellenberg J, Foisner R, Noegel AA, Karakesisoglou I. 2008. Sun1 forms immobile macromolecular assemblies at the nuclear envelope. Biochim Biophys Acta 1783:2415–2426. https://doi.org/10.1016/j.bbamcr.2008.09.001.

53. Haque F, Mazzeo D, Patel JT, Smallwood DT, Ellis JA, Shanahan CM, Shackleton S. 2010. Mammalian SUN protein interaction networks at the inner nuclear membrane and their role in laminopathy disease processes. J Biol Chem 285:3487–3498. https://doi.org/10.1074/jbc.M109.071910.

54. Jahed Z, Fadavi D, Vu UT, Asgari E, Luxton GWG, Mofrad MRK. 2018. Molecular insights into the mechanisms of SUN1 oligomerization in the nuclear envelope. Biophys J 114:1190–1203. https://doi.org/10.1016/j.bpj.2018.01.015.

55. Porter L, Minaisah RM, Ahmed S, Ali S, Norton R, Zhang Q, Ferraro E, Molenaar C, Holt M, Cox S, Fountain S, Shanahan C, Warren D. 2020. SUN1/2 are essential for RhoA/ROCK-regulated actomyosin activity in isolated vascular smooth muscle cells. Cells 9:132. https://doi.org/10.3390/cells9010132.

56. Lei K, Zhang X, Ding X, Guo X, Chen M, Zhu B, Xu T, Zhuang Y, Xu R, Han M. 2009. SUN1 and SUN2 play critical but partially redundant roles in anchoring nuclei in skeletal muscle cells in mice. Proc Natl Acad Sci U S A 106:10207–10212. https://doi.org/10.1073/pnas.0812037106.

57. Ostlund C, Folker ES, Choi JC, Gomes ER, Gundersen GG, Worman HJ. 2009. Dynamics and molecular interactions of linker of nucleoskeleton and cytoskeleton (LINC) complex proteins. J Cell Sci 122:4099–4108. https://doi.org/10.1242/jcs.057075.

58. Liang Y, Chiu PH, Yip KY, Chan SY. 2011. Subcellular localization of SUN2 is regulated by lamin A and Rab5. PLoS One 6:e20507. https://doi.org/10.1371/journal.pone.0020507.

59. Liang WC, Mitsuhashi H, Keduka E, Nonaka I, Noguchi S, Nishino I, Hayashi YK. 2011. TMEM43 mutations in Emery-Dreifuss muscular dystrophy-related myopathy. Ann Neurol 69:1005–1013. https://doi.org/10.1002/ana.22338.

60. Loret S, Guay G, Lippé R. 2008. Comprehensive characterization of extracellular herpes simplex virus type 1 virions. J Virol 82:8605–8618. https://doi.org/10.1128/JVI.00904-08.

61. Yuan W, Song C. 2020. The emerging role of Rab5 in membrane receptor trafficking and signaling pathways. Biochem Res Int 2020:4186308. https://doi.org/10.1155/2020/4186308.

62. Hollinshead M, Johns HL, Sayers CL, Gonzalez-Lopez C, Smith GL, Elliott G. 2012. Endocytic tubules regulated by Rab GTPases 5 and 11 are used for envelopment of herpes simplex virus. EMBO J 31:4204–4220. https://doi.org/10.1038/emboj.2012.262.

63. Boruchowicz H, Hawkins J, Cruz-Palomar K, Lippé R. 2020. The XPO6 exportin mediates HSV-1 gM nuclear release late in infection. J Virol 94:e00753-20. https://doi.org/10.1128/JVI.00753-20.

64. Vander Heyden AB, Naismith TV, Snapp EL, Hodzic D, Hanson PI. 2009. LULL1 retargets TorsinA to the nuclear envelope revealing an activity that is impaired by the DYT1 dystonia mutation. Mol Biol Cell 20:2661–2672. https://doi.org/10.1091/mbc.e09-01-0094.

65. Holper JE, Klupp BG, Luxton GWG, Franzke K, Mettenleiter TC. 2020. Function of Torsin AAA+ ATPases in pseudorabies virus nuclear egress. Cells 9:738. https://doi.org/10.3390/cells9030738.

66. Donahue DA, Amraoui S, di Nunzio F, Kieffer C, Porrot F, Opp S, Diaz-Griffero F, Casartelli N, Schwartz O. 2016. SUN2 overexpression deforms nuclear shape and inhibits HIV. J Virol 90:4199–4214. https://doi.org/10.1128/JVI.03202-15.

67. Donahue DA, Porrot F, Couespel N, Schwartz O. 2017. SUN2 silencing impairs CD4 T cell proliferation and alters sensitivity to HIV-1 infection independently of cyclophilin A. J Virol 91:e02303-16. https://doi.org/10.1128/JVI.02303-16.

68. Dull T, Zufferey R, Kelly M, Mandel RJ, Nguyen M, Trono D, Naldini L. 1998. A third-generation lentivirus vector with a conditional packaging system. J Virol 72:8463–8471. https://doi.org/10.1128/JVI.72.11.8463-8471.1998.

69. Sakuma T, Barry MA, Ikeda Y. 2012. Lentiviral vectors: basic to translational. Biochem J 443:603–618. https://doi.org/10.1042/BJ20120146.

70. Das AT, Tenenbaum L, Berkhout B. 2016. Tet-On systems for doxycycline-inducible gene expression. Curr Gene Ther 16:156–167. https://doi.org/10.2174/1566523216666160524144041.

71. Backman CM, Zhang Y, Hoffer BJ, Tomac AC. 2004. Tetracycline-inducible expression systems for the generation of transgenic animals: a comparison of various inducible systems carried in a single vector. J Neurosci Methods 139:257–262. https://doi.org/10.1016/j.jneumeth.2004.05.012.

72. Gibson DG. 2011. Enzymatic assembly of overlapping DNA fragments. Methods Enzymol 498:349–361. https://doi.org/10.1016/B978-0-12-385120-8.00015-2.